Nonlinear Dynamics (2006) 43: 73–96

Modelling, Dynamics and Control of Tethered Satellite Systems

M. KRUPA, W. POTH, M. SCHAGERL, A. STEINDL, W. STEINER, H. TROGER*, and G. WIEDERMANN
Institute for Mechanics, Vienna University of Technology, Austria;
**Author for correspondence (e-mail: hans.troger@tuwien.ac.at; fax: ++431 58801 32598)*

(Received: 1 March 2004; accepted: 2 December 2004)

Abstract. Tethered satellite systems (TSS) pose quite challenging problems concerning their modelling, derivation of the equations of motion, numerical simulation of their dynamics, deciding on stability of relative equilibria provided the system moves on a circular orbit around the Earth and the occurrence of chaotic dynamics. Moreover, for the processes of deployment or retrieval of one satellite from or to another satellite certain control strategies, for example time or energy optimal control, are necessary. All these problems are considered in this paper.

Key words: chaotic dynamics, Hamilton's principle, optimal control, reduced energy momentum method, relative equilibrium, stiff differential equations

1. Introduction

The concept of tethered satellite systems (TSS), that is, two or more satellites in orbit connected by thin long cables – a length of 100 km is not unusual – is probably the most innovative concept of space flight at the end of the 20th century (see for an extensive introduction into this subject: [1–4]) because there exist numerous important applications [3] ranging from energy production, making use of the magnetic field of the Earth, to orbit raising or deorbiting of satellites just by cutting the tether. Already several flights in orbit around the Earth, organized by NASA, were performed during the last decade of the 20th century.

In this paper, we want to discuss a selected number of interesting problems that arise in the treatment of such systems. We start with modelling. Then, we focus on some problems related to the variational formulation of the equations of motion. Concerning the numerical solution procedure by Finite Elements we compare the usually used displacement coordinates with an alternative set of variables called Minakov's variables in [3], which turns out to be superior for the effective numerical integration of the mathematically stiff system of partial and ordinary differential equations if the tether is physically very stiff.

We also address three other questions that are of great theoretical and practical importance. One is stability of relative equilibria, if the system is moving on a circular orbit. Since a continuous system is considered, this requires the use of advanced mathematical methods, which are supplied by the Reduced Energy Momentum Method [5–8]. The second is the occurence of chaotic dynamics which is also of great practical interest, because the sensitive dependence of final states on initial conditions may have the consequence that comparing the results of different simulation programs might lead to conclusions that the codes do not work well. But here the theoretically well known consequences concerning numerical simulation of chaotic dynamics should be taken into account. Thirdly, and finally, in order to bring a

system in its operational state into orbit, deployment and possibly also retrieval of one satellite from or to another must be performed. These are important processes but also delicate operations for a tethered satellite system mission because both processes lead to unstable motions with respect to the stable radial relative equilibrium configuration of such a system, which is attained if it is moving with constant tether length on a Keplerian circle around the Earth. Therefore, we propose for the system motion on a Keplerian circle a deployment or retrieval strategy which guarantees a time optimal deployment or retrieval process from the radial relative equilibrium position close to the main satellite to the radial relative equilibrium position far away from the main satellite in deployment, and vice versa for retrieval. It is important to mention that this is achieved only by tension control, that is the control acts on the system only by varying the tension in the tether at the tether feed-out point at one of the satellites.

2. Mechanical Model and Equations of Motion

The tether is modelled as a perfectly flexible, massive, continuous, visco-elastic string with variable length [3, 9, 10]. The endbodies are modelled either as point masses or rigid bodies [3, 11]. In [12] simulation results are presented that indicate that for the study of the overall motions of long tethers with small endbodies the influence of the rigid body rotations on the motion of the tether is negligible. This means that if the rotational motion of the endbodies is not of interest, mass points are a good mechanical model. An important question is how the tether storage in the satellites should be modelled, and how the processes of deployment and retrieval should be described dynamically. In a simplified, but still quite accurate modelling, the details of the deployment mechanism are not taken into account and it is assumed that the tether is stowed as point mass, which is at rest relative to the body in which it is stored [13]. More complicated storage models have also been studied, where, for example the tether is stored on a drum [14].

2.1. Derivation of the Equations of Motion from Balance Principles

Equations of motion have been formulated either starting from balance principles or variational principles [15]. They are a set of coupled nonlinear ordinary and partial differential equations. Since the deployed length of the tether may vary during a mission (deployment and retrieval), the partial differential equation is defined on a domain, the length of which is unknown and must itself be determined by the solution of the problem. Using a variational principle for the derivation of the equations of motion is of advantage for their numerical treatment by a Finite Element discretization and also supplies the correct boundary conditions, but raises new problems following from the variable length of the domain, because it introduces additional non-conservative terms.

The motion of the tether is described by the partial differential equation

$$\mu \ddot{\boldsymbol{r}} = \boldsymbol{n}' + \boldsymbol{f}_{\mathrm{T}}. \tag{1}$$

Here $\boldsymbol{r}$ is the position vector in the inertial frame located in the center of the Earth (Figure 1). $(\,)^{\cdot}$ denotes the derivative with respect to time t. μ is the mass density of the tether per unit unstrained arc-length s, which is considered as a material coordinate. $(\,)'$ denotes the derivative with respect to the unstrained arc-length s. By $\hat{s}$ we will denote the strained or actual arc-length. For the extensible tether we have to distinguish between the unstrained arc-length s and the actual arc-length $\hat{s}$. In the formulation given below the unstrained arclength s with $0 \leq s \leq l$ is used. The advantage of this choice is that then the

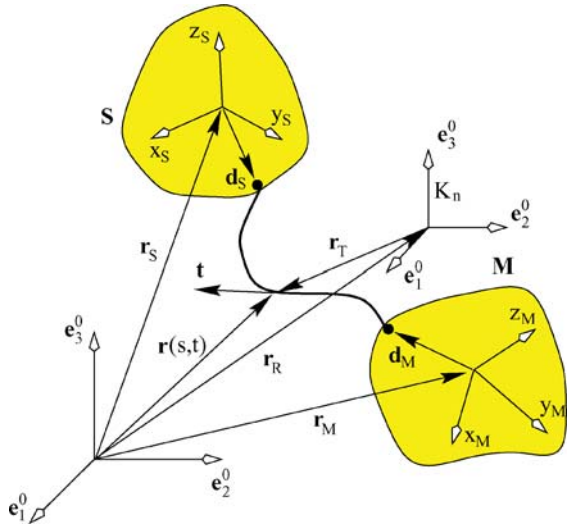

Figure 1. Two tethered satellites and the local non-rotating floating frame K_n. The two dots represent the amount of tether stored in the satellites.

boundary conditions are given for the values of the unstrained arc-length. We subdivide the tether length l into three domains

$$\begin{aligned} 0 \le s &\le s_M(t) \\ s_M(t) \le s &\le s_S(t) \\ s_S(t) \le s &\le l \end{aligned} \tag{2}$$

Tether of length s_M is stored in satellite M and of length $l - s_S$ in satellite S. The remaining part of length $s_S - s_M$ is deployed between the two satellites. $\boldsymbol{n}$ is the axial force in the tether. $\boldsymbol{f}_T$ is the vector of distributed forces acting on the tether element. As a constitutive relation for the string we assume a material law in the form

$$N = N(\varepsilon, \dot{\varepsilon}), \tag{3}$$

relating the value of the tether force N to the strain ε. This form of the constitutive law includes the linear Kelvin1–Voigt law of visco-elasticity

$$N = EA(\varepsilon + \alpha\dot{\varepsilon}). \tag{4}$$

Here E is Young's modulus, A is the area of the cross-section of the string. Hence, the axial force $\boldsymbol{n}$ in the string follows from (3) to

$$\boldsymbol{n} = N\boldsymbol{t}, \tag{5}$$

where $\boldsymbol{t}$ is the tangent vector to the string. For ε we obtain

$$\varepsilon = \frac{d\hat{s} - ds}{ds} = \eta - 1 = \|\boldsymbol{r}'\| - 1. \tag{6}$$

where η is the elongation. The last relation in (6) follows from the fact that the tangent vector

$$\boldsymbol{t} = \frac{\partial \boldsymbol{r}}{\partial \hat{s}} = \frac{1}{\eta}\boldsymbol{r}' \tag{7}$$

is a unit vector. From $\boldsymbol{t} \cdot \boldsymbol{t} = 1$ immediately follows $\eta = \|\boldsymbol{r}'\|$. If we rewrite (4) with η as variable we obtain

$$\begin{aligned} N &= EA(\|\boldsymbol{r}'\| - 1 + \alpha \dot{\boldsymbol{r}}' \cdot \boldsymbol{t}) = EA(\eta - 1 + \alpha\dot{\eta}) \\ &= N_{\mathrm{C}}(\eta(s,t), s) + N_{\mathrm{D}}(\dot{\eta}(s,t), s). \end{aligned} \tag{8}$$

In addition we have the kinematic relationship (Figure 1) (expressions for satellite S that are analogous to those for satellite M will not be given explicitly for the following equations)

$$\boldsymbol{r}(s_{\mathrm{M}}(t), t) = \boldsymbol{r}_{\mathrm{M}}(t) + \boldsymbol{d}_{\mathrm{M}}(t). \tag{9}$$

The boundary conditions at the ends of the deployed tether are determined by the motions of the two satellites given by the linear and angular momentum equations. The linear momentum balance yields

$$m^0_{\mathrm{M}}\ddot{\boldsymbol{r}}_{\mathrm{M}} + \mu s_{\mathrm{M}}\ddot{\boldsymbol{r}}_{\mathrm{M}} + \mu \dot{s}^2_{\mathrm{M}}\boldsymbol{r}'(s_{\mathrm{M}}) = \boldsymbol{f}_{\mathrm{M}} + \boldsymbol{n}(s_{\mathrm{M}}). \tag{10}$$

Further m^0_{M} is the satellite mass without the mass of the stored tether. The third term on the left hand side of (10) is a so-called rocket term and results from the fact that the mass of the satellite is variable. $\boldsymbol{f}_{\mathrm{M}}$ is the vector of all external forces acting on endbody M. In writing down the angular momentum balance we use the notation introduced in [16] where the same quantity measured in the inertial frame and in the moving frame is denoted by the same letter but lower and upper case, respectively. These quantities are related to each other by the rotation matrix $\mathbf{B}$. For example, we obtain for the resultant external moment acting on body M: $\boldsymbol{m}_{\mathrm{M}} = \mathbf{B}_{\mathrm{M}}\boldsymbol{M}_{\mathrm{M}}$ where $\mathbf{B}_{\mathrm{M}}$ is the rotation matrix between the body fixed frame and the inertial frame. The angular momentum balance results in

$$\mathbf{I}^0_{\mathrm{M}}\dot{\boldsymbol{\Omega}}_{\mathrm{M}} + \boldsymbol{\Omega}_{\mathrm{M}} \times \left(\mathbf{I}^0_{\mathrm{M}}\boldsymbol{\Omega}_{\mathrm{M}}\right) + \boldsymbol{D}_{\mathrm{M}} \times \mathbf{B}^{\mathrm{T}}_{\mathrm{M}}\left(\mu s_{\mathrm{M}}\ddot{\boldsymbol{r}}_{\mathrm{S}} + \mu \dot{s}^2_{\mathrm{M}}\boldsymbol{r}'(s_{\mathrm{M}}) - \boldsymbol{n}(s_{\mathrm{M}})\right) = \boldsymbol{M}_{\mathrm{M}} \tag{11}$$

where $\mathbf{I}^0_{\mathrm{M}}$ is the inertia tensor of satellite M without the stored part of the tether. $\boldsymbol{\Omega}_{\mathrm{M}}$ is the angular velocity in the body-fixed coordinate frame. $\boldsymbol{D}_{\mathrm{M}}$ denotes the distance from the mass center of the satellite to the point where the tether is stored in the satellite measured in the body fixed frame. $\boldsymbol{d}_{\mathrm{M}}$ is the same quantity measured in the inertial frame. These two quantities are related to each other by

$$\boldsymbol{d}_{\mathrm{M}} = \mathbf{B}_{\mathrm{M}}\boldsymbol{D}_{\mathrm{M}}. \tag{12}$$

The relation between $\boldsymbol{\Omega}_{\mathrm{M}}$ and $\mathbf{B}_{\mathrm{M}}$ is given by (the hat denotes the skew symmetric matrix corresponding to the vector)

$$\hat{\boldsymbol{\Omega}}_{\mathrm{M}} = \mathbf{B}^{\mathrm{T}}_{\mathrm{M}}\dot{\mathbf{B}}_{\mathrm{M}} = \begin{pmatrix} 0 & -\Omega_3 & \Omega_2 \\ \Omega_3 & 0 & -\Omega_1 \\ -\Omega_2 & \Omega_1 & 0 \end{pmatrix}. \tag{13}$$

The external forces ($\boldsymbol{f}_\mathrm{T}$, $\boldsymbol{f}_\mathrm{M}, \ldots$) and moments ($\boldsymbol{M}_\mathrm{M}, \ldots$) follow from various sources such as gravitational attractions of various planets, aerodynamic effects, electromagnetic effects, solar radiation pressure and perhaps thrusters used for control purposes to mention some [3].

If we count the unknowns we find that there are nine vectorial and two scalar quantities: $\boldsymbol{r}(s,t), \boldsymbol{r}_\mathrm{M}(t), \boldsymbol{r}_\mathrm{S}(t), \boldsymbol{d}_\mathrm{M}(t), \boldsymbol{d}_\mathrm{S}(t)\ \mathbf{B}_\mathrm{M}, \mathbf{B}_\mathrm{S}, \boldsymbol{\Omega}_\mathrm{M}, \boldsymbol{\Omega}_\mathrm{S}, s_\mathrm{M}(t)$ and $s_\mathrm{S}(t)$.

So far we have the following equations: One vectorial field Equation (1), two vectorial linear momentum Equations (10) and two vectorial angular momentum Equations (11), and two vectorial equations for each satellite given by (12) and (13), which makes nine vectorial equations. However, two scalar equations are missing which relate the length change of the tether at the satellites to the forces acting there. They are derived in the following section for tether storage on a spool. For tether storage on a drum we refer to [14, 17].

2.2. Deployment and Retrieval Dynamics

During deployment or retrieval the arc-length coordinates $s = s_\mathrm{M}(t)$ and $s = s_\mathrm{S}(t)$ at the satellites move along the configuration of the tether. Hence, the masses of the endbodies change. The tensions $N(s_\mathrm{M}^+)$ and $N(s_\mathrm{S}^-)$ (and therefore the axial forces $\boldsymbol{n}(s_\mathrm{M}^+) = N(s_\mathrm{M}^+)\boldsymbol{t}$ and $\boldsymbol{n}(s_\mathrm{S}^-) = N(s_\mathrm{S}^-)\boldsymbol{t}$) in the tether at the feed-out points depend on the deployment mechanisms inside the satellites.

2.2.1. *Deployment Mechanism*

Since the results for the two satellites are analogous with $s_\mathrm{M} \leftrightarrow l - s_\mathrm{S}$ we consider only the satellite M. The linear momentum balance of a tether element at $s = s_\mathrm{M}(t)$ yields [14]

$$N_\mathrm{M} = N(s_\mathrm{M}^+) - N(s_\mathrm{M}^-) + \mu \dot{s}_\mathrm{M}[\dot{\boldsymbol{r}}(s_\mathrm{M}^+) - \dot{\boldsymbol{r}}(s_\mathrm{M}^-)] \cdot \boldsymbol{t}(s_\mathrm{M}) \tag{14}$$

where N_M is the force shown in Figure 2a acting on the tether at the tether outlet of the satellite. The presented models are physically reasonable, but they do not conserve energy, which, as already mentioned, creates problems in the derivation of the equation of motion by means of a variational principle [18].

Spool Deployer. We assume the following mechanism for $\dot{s}_\mathrm{M} \leq 0$ (Figure 2a): The relaxed tether is stored inside the satellite, $N(s_\mathrm{M}^-) = 0$. Due to the tension $N(s_\mathrm{M}^+)$ it is instantaneously accelerated from $\dot{\boldsymbol{r}}_\mathrm{M}$ to $\dot{\boldsymbol{r}}(s_\mathrm{M}^+)$ by the value

$$v_\mathrm{rel} = [\dot{\boldsymbol{r}}(s_\mathrm{M}^+) - \dot{\boldsymbol{r}}_\mathrm{M}] \cdot \boldsymbol{t}(s_\mathrm{M}) = -\dot{s}_\mathrm{M}\, \eta(s_\mathrm{M}^+)$$

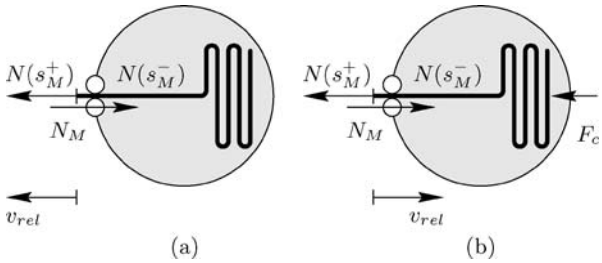

Figure 2. Endbody with spool deployer (a). In case of retrieval (b) the string is pulled into the satellite by N_M and stopped by the internal constraint force F_c.

which follows from differentiating $\boldsymbol{r}_{\mathrm{M}}(t) = \boldsymbol{r}(s_{\mathrm{M}}^{+}, t)$ and then using the relation (7). This discontinuous change of the state may, if present, be braked by the force N_{M}. Then, the jump condition (14) yields

$$N(s_{\mathrm{M}}^{+}) = N_{\mathrm{M}} + \mu \dot{s}_{\mathrm{M}}^{2}\, \eta(s_{\mathrm{M}}^{+}). \tag{15}$$

Spool Retriever. In case of retrieval $\dot{s}_{\mathrm{M}} \geq 0$ the tether is pulled inside the satellite by the force N_{M} (Figure 2b). If we assume that such a mechanism is realized by small rolls it is evident that the tether is relaxed after arriving in the satellite, hence, $N(s_{\mathrm{M}}^{-}) = 0$. Under this assumption the elongation jumps from $\eta(s_{\mathrm{M}}^{+})$ to the value $\eta(s_{\mathrm{M}}^{-}) = 1$ and the jump condition therefore yields

$$\begin{aligned} N(s_{\mathrm{M}}^{+}) &= N_{\mathrm{M}} - \mu \dot{s}_{\mathrm{M}}[\dot{\boldsymbol{r}}(s_{\mathrm{M}}^{+}) - \dot{\boldsymbol{r}}(s_{\mathrm{M}}^{-})] \cdot \boldsymbol{t}(s_{\mathrm{M}}) \\ &= N_{\mathrm{M}} + \mu \dot{s}_{\mathrm{M}}^{2}[\eta(s_{\mathrm{M}}^{+}) - 1]. \end{aligned} \tag{16}$$

In an impact the (now unstrained) tether is decelerated to the satellites velocity $\dot{\boldsymbol{r}}_{\mathrm{M}}$ by the internal constraint force

$$F_{\mathrm{c}} = \mu \dot{s}_{\mathrm{M}}[\dot{\boldsymbol{r}}(s_{\mathrm{M}}^{-}) - \dot{\boldsymbol{r}}_{\mathrm{M}}] \cdot \boldsymbol{t}(s_{\mathrm{M}}) = \mu \dot{s}_{\mathrm{M}}^{2}$$

which, however, is already included in the linear momentum balance [18].

2.3. Equations of Motion Derived from a Variational Principle

We use the variational principle of Hamilton Ostrogradski [19] in the form

$$\int_{t_0}^{t_1} (\delta T - \delta V + \delta' W)\, dt = 0, \tag{17}$$

where T is the kinetic energy, V the potential energy and $\delta' W$ takes care of all effects which cannot be derived from a potential. Specifically these expressions are

$$\begin{aligned} T &= \int_{s_{\mathrm{M}}}^{s_{\mathrm{S}}} \frac{1}{2}\mu \dot{\boldsymbol{r}}^{2}\, ds + \frac{1}{2} m_{\mathrm{M}}^{0} \dot{\boldsymbol{r}}_{\mathrm{M}}^{2} + \frac{1}{2} m_{\mathrm{S}}^{0} \dot{\boldsymbol{r}}_{\mathrm{S}}^{2} + \frac{1}{2}\mu s_{\mathrm{M}} \dot{\boldsymbol{r}}_{\mathrm{M}}^{2} + \frac{1}{2}\mu (l - s_{\mathrm{S}})\, \dot{\boldsymbol{r}}_{\mathrm{S}}^{2}, \\ V &= \int_{s_{\mathrm{M}}}^{s_{\mathrm{S}}} (\Pi + \mu\Phi)\, ds + m_{\mathrm{M}}^{0} \Phi(\boldsymbol{r}_{\mathrm{M}}) + m_{\mathrm{S}}^{0} \Phi(\boldsymbol{r}_{\mathrm{S}}) + \mu s_{\mathrm{M}} \Phi(\boldsymbol{r}_{\mathrm{S}}) + \mu (l - s_{\mathrm{S}}) \Phi(\boldsymbol{r}_{\mathrm{S}}), \\ \delta' W &= \int_{s_{\mathrm{M}}}^{s_{\mathrm{S}}} (-N_{\mathrm{D}} \delta\eta + \boldsymbol{f}_{T_{\mathrm{D}}} \cdot \delta\boldsymbol{r})\, ds + \boldsymbol{f}_{M_{\mathrm{D}}} \cdot \delta\boldsymbol{r}_{\mathrm{M}} + \boldsymbol{f}_{S_{\mathrm{D}}} \cdot \delta\boldsymbol{r}_{\mathrm{S}} \\ &\quad + \mathrm{CELT}_{\mathrm{M}} \delta s_{\mathrm{M}} + \mathrm{CELT}_{\mathrm{S}} \delta s_{\mathrm{S}} + N_{\mathrm{M}} \eta(s_{\mathrm{M}}) \delta s_{\mathrm{M}} - N_{\mathrm{S}} \eta(s_{\mathrm{S}}) \delta s_{\mathrm{S}}. \end{aligned} \tag{18}$$

The strain energy and the dissipative part in the material law are defined by

$$\begin{aligned} \Pi(\eta(s,t), s) &= \int_{1}^{\eta} N_{\mathrm{C}}(v, s)\, dv, \quad \delta\Pi = \frac{\partial \Pi}{\partial \eta} \delta\eta = N_{\mathrm{C}} \delta\eta, \\ \delta\eta &= \boldsymbol{t} \cdot \delta\boldsymbol{r}', \quad \delta' W_{\mathrm{N}} = -(N_{\mathrm{C}} + N_{\mathrm{D}}) \delta\eta = -\boldsymbol{n} \cdot \delta\boldsymbol{r}', \end{aligned}$$

Specializing for the linear visco-elastic material we obtain

$$N_{\mathrm{C}} = EA(\eta - 1), \quad N_{\mathrm{D}} = EA\alpha\dot{\eta}, \quad \Pi = \frac{1}{2}EA(\eta - 1)^2,$$

or inserting above for η according to (6) we obtain

$$\begin{aligned} N &= EA(\|\boldsymbol{r}'\| - 1 + \alpha\dot{\boldsymbol{r}}' \cdot \boldsymbol{t}) = EA(\eta - 1 + \alpha\dot{\eta}) \\ &= N_{\mathrm{C}}(\eta(s,t), s) + N_{\mathrm{D}}(\dot{\eta}(s,t), s). \end{aligned}$$

Due to the discontinuity of speed and tension in the tether at the feed-out points the process of changing mass as modelled here is not energy conserving, as mentioned before. In order to still be able to derive the equations of motion from a variational principle proper terms must be introduced, which we call Carnot energy loss term (CELT) following [20]. In [18] it is explained how they can be calculated. They are for deployment from a spool

$$\begin{aligned} \mathrm{CELT}_{\mathrm{M}} &= \frac{1}{2}\mu\dot{s}_{\mathrm{M}}^2\eta^2(s_{\mathrm{M}}) - \Pi(s_{\mathrm{M}}), \\ \mathrm{CELT}_{\mathrm{S}} &= -\frac{1}{2}\mu\dot{s}_{\mathrm{S}}^2\eta^2(s_{\mathrm{S}}) + \Pi(s_{\mathrm{S}}), \end{aligned}$$

and for retrieval on a spool

$$\begin{aligned} \mathrm{CELT}_{\mathrm{M}} &= -\frac{1}{2}\mu\dot{s}_{\mathrm{M}}^2\eta(s_{\mathrm{M}})(2 - \eta(s_{\mathrm{M}})) - \Pi(s_{\mathrm{M}}), \\ \mathrm{CELT}_{\mathrm{S}} &= \frac{1}{2}\mu\dot{s}_{\mathrm{S}}^2\eta(s_{\mathrm{S}})(2 - \eta(s_{\mathrm{S}})) + \Pi(s_{\mathrm{S}}). \end{aligned}$$

Inserting into (17) we first perform the partial integration with respect to time t. This is a nontrivial operation due to the fact that $s_{\mathrm{M}}(t)$ and $s_{\mathrm{S}}(t)$ are variables and not prescribed in time. The necessary calculations are explained in detail in [14]. As result we obtain the functional

$$\begin{aligned} G = \int_{t_0}^{t_1} \Bigg\{ & \int_{s_{\mathrm{M}}}^{s_{\mathrm{S}}} \left\{ \left[-\mu(\ddot{\boldsymbol{r}} + \nabla\Phi) + \boldsymbol{f}_{T_{\mathrm{D}}} \right] \cdot \delta\boldsymbol{r} - \boldsymbol{n} \cdot \delta\boldsymbol{r}' \right\} ds \\ & + \begin{cases} \left[\mu\dot{s}_{\mathrm{M}}^2\eta^2(s_{\mathrm{M}}) + N_{\mathrm{M}}\eta(s_{\mathrm{M}}) \right] \delta s_{\mathrm{M}} & \text{Deployment} \\ \left[\mu\dot{s}_{\mathrm{M}}^2\eta(s_{\mathrm{M}})(\eta(s_{\mathrm{M}}) - 1) + N_{\mathrm{M}}\eta(s_{\mathrm{M}}) \right] \delta s_{\mathrm{M}} & \text{Retrieval} \end{cases} \\ & + \begin{cases} \left[-\mu\dot{s}_{\mathrm{S}}^2\eta^2(s_{\mathrm{S}}) - N_{\mathrm{S}}\eta(s_{\mathrm{S}}) \right] \delta s_{\mathrm{S}} & \text{Deployment} \\ \left[\mu\dot{s}_{\mathrm{S}}^2\eta(s_{\mathrm{S}})(\eta(s_{\mathrm{S}}) - 1) - N_{\mathrm{S}}\eta(s_{\mathrm{S}}) \right] \delta s_{\mathrm{S}} & \text{Retrieval} \end{cases} \\ & + \left[-m_{\mathrm{M}}^0(\ddot{\boldsymbol{r}}_{\mathrm{M}} + \nabla\Phi(\boldsymbol{r}_{\mathrm{M}})) - \mu s_{\mathrm{M}}(\ddot{\boldsymbol{r}}_{\mathrm{S}} + \nabla\Phi(\boldsymbol{r}_{\mathrm{S}})) - \mu\dot{s}_{\mathrm{M}}^2\boldsymbol{r}'(s_{\mathrm{M}}) + \boldsymbol{f}_{M_{\mathrm{D}}} \right] \cdot \delta\boldsymbol{r}_{\mathrm{M}} \\ & + \left[-m_{\mathrm{S}}^0(\ddot{\boldsymbol{r}}_{\mathrm{M}} + \nabla\Phi(\boldsymbol{r}_{\mathrm{S}})) - \mu(l - s_{\mathrm{S}})(\ddot{\boldsymbol{r}}_{\mathrm{S}} + \nabla\Phi(\boldsymbol{r}_{\mathrm{S}})) + \mu\dot{s}_{\mathrm{S}}^2\boldsymbol{r}'(s_{\mathrm{S}}) + \boldsymbol{f}_{S_{\mathrm{D}}} \right] \cdot \delta\boldsymbol{r}_{\mathrm{S}} \\ & + \left\{ -\mathbf{I}_{\mathrm{M}}^0\dot{\boldsymbol{\Omega}}_{\mathrm{M}} - \boldsymbol{\Omega}_{\mathrm{M}} \times \left(\mathbf{I}_{\mathrm{M}}^0\boldsymbol{\Omega}_{\mathrm{M}} \right) + \boldsymbol{M}_{M_{\mathrm{D}}} \right. \\ & \left. + \boldsymbol{D}_{\mathrm{M}} \times \mathbf{B}_{\mathrm{M}}^{\mathrm{T}} \left[-\mu s_{\mathrm{M}}(\ddot{\boldsymbol{r}}_{\mathrm{S}} + \nabla\Phi(\boldsymbol{r}_{\mathrm{S}})) - \mu\dot{s}_{\mathrm{M}}^2\boldsymbol{r}'(s_{\mathrm{M}}) \right] \right\} \cdot \delta\Theta_{\mathrm{M}} \\ & + \left\{ -\mathbf{I}_{\mathrm{S}}^0\dot{\boldsymbol{\Omega}}_{\mathrm{S}} - \boldsymbol{\Omega}_{\mathrm{S}} \times \left(\mathbf{I}_{\mathrm{S}}^0\boldsymbol{\Omega}_{\mathrm{S}} \right) + \boldsymbol{M}_{S_{\mathrm{D}}} \right. \\ & \left. + \boldsymbol{D}_{\mathrm{S}} \times \mathbf{B}_{\mathrm{S}}^{\mathrm{T}} \left[-\mu(l - s_{\mathrm{S}})(\ddot{\boldsymbol{r}}_{\mathrm{S}} + \nabla\Phi(\boldsymbol{r}_{\mathrm{S}})) + \mu s_{\mathrm{S}}^2\boldsymbol{r}'(s_{\mathrm{S}}) \right] \right\} \cdot \delta\Theta_{\mathrm{S}} \Bigg\} dt = 0. \end{aligned} \tag{19}$$

Here $\nabla\Phi(\boldsymbol{r})$ is given by $-\nabla\Phi(\boldsymbol{r}) = -\mu_{\mathrm{E}}\frac{\boldsymbol{r}}{\|\boldsymbol{r}\|^3}$. μ_{E} is the gravitational constant of the Earth. Concerning the Carnot energy loss concept we refer to [18], where an extensive treatment has been given by means of simple examples.

2.4. Equations of Motion Given in Natural String Coordinates

Since practically used tethers, compared to the acting forces, are very stiff axially, the equations are stiff in mathematical respect. This property, if not taken into account properly, may result in problems for an efficient numerical integration [21]. In this context stiff means that motions in the system dynamics are present which evolve on different time scales as it is shown for the simple string pendulum in Figure 3. From Figure 3 it is easy to understand that the motion of a TSS can be split into very fast oscillations in axial direction of the tether and into two comparably slow oscillations in transverse direction. One is the oscillation of the tether in the direction transversal to its tangent. The other is the overall pendulum-like oscillation of the whole system which is also slowly evolving. In order to integrate a stiff system in a numerically efficient way two aspects are important. First the selection of an appropriate time integrator and second a proper choice of variables in the description of the deformation of the tether. Concerning the first point implicit integration schemes must be selected [22]. Concerning the second point already in [3, 21, 23] an alternative formulation of the equations of motion is proposed. Here as variables – contrary to the usual displacement formulation – so-called natural string coordinates, namely, the orientation of the tangent vector $\boldsymbol{t}$ to the deformed tether and the elongation η of the tether (or the strain ε) are used (Figure 4). We indicate below that with respect to leading derivatives the equations of motion naturally split into a stiff part and into a non-stiff part. After discretization of the continuous tether in space by Finite Elements or Finite Differences a set of nonlinear ordinary differential equations is obtained, which takes the form of a singularly perturbed system

$$\begin{aligned} \dot{\boldsymbol{\Phi}} &= \boldsymbol{f}(t, \boldsymbol{\Phi}, \boldsymbol{H}, \nu), \\ \nu\dot{\boldsymbol{H}} &= \boldsymbol{g}(t, \boldsymbol{\Phi}, \boldsymbol{H}, \nu). \end{aligned} \tag{20}$$

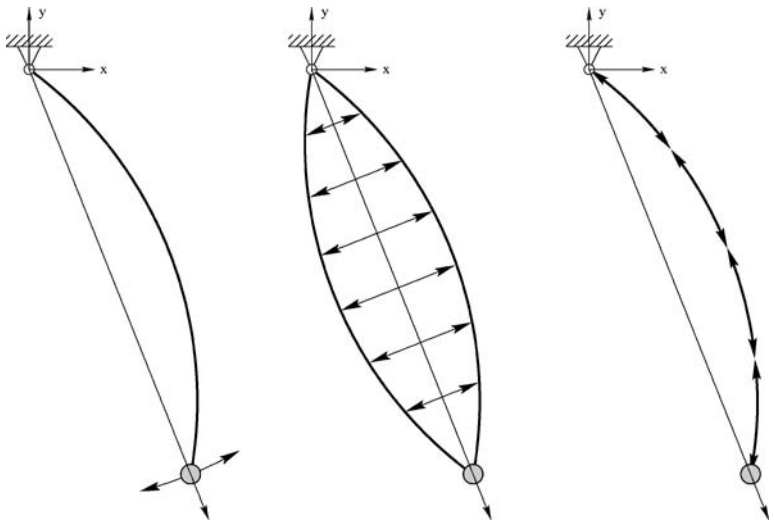

Figure 3. Explanation of the fast and slow motions in a mathematically stiff system: left and middle frame show the slow transversal motions whereas in the right frame the fast axial motion is shown.

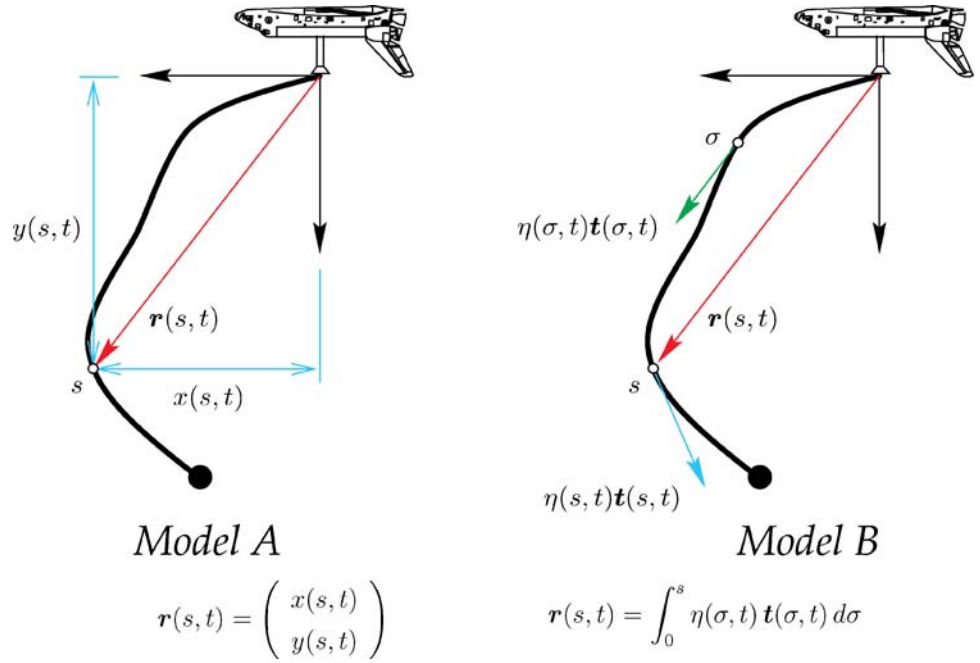

Figure 4. The planar deformation of the tether $\boldsymbol{r}(s,t)$ may be described either by its Cartesian components (model A) or by natural string coordinates (model B).

In (20) ν is a small parameter which is proportional to $1/EA$, where EA is the axial stiffness of the tether (E is Young's modulus and A the constant area of the tether's cross-section) and $\boldsymbol{\Phi}$, $\boldsymbol{H}$ are vectors obtained after discretization. In (20) also the transition to a differential algebraic system is obvious if one lets $EA \to \infty$ which is equivalent to $\nu \to 0$.

We indicate the structure of the equations of motion using as variables the elongation of the tether and the orientation of the tangent vector to the tether (Figure 4, model B) following the derivation given in [3] resulting in a set of equations named *Minakov's equations*. The position vector $\boldsymbol{r}(s,t)$ now will be represented by the tangential vector $\boldsymbol{t}$ and the elongation η. This is achieved by integration of (7) with respect to the unstrained arc-length s yielding

$$\boldsymbol{r}(s,t) = \int_0^s \eta(\sigma,t)\boldsymbol{t}(\sigma,t)\,d\sigma\ . \tag{21}$$

In (21) the inextensional case is given by setting $\eta = 1$.

In order to obtain equations for $\boldsymbol{t}$ and η we differentiate (1) with respect to s to obtain

$$\ddot{\boldsymbol{r}}' = \frac{1}{\mu}(N\boldsymbol{t})'' - (\nabla\Phi(\boldsymbol{r}))' + \frac{1}{\mu}(\boldsymbol{f})' \tag{22}$$

Substituting from (7) for $\boldsymbol{r}'$ into (22) yields

$$(\eta\boldsymbol{t})\ddot{} = \frac{1}{\mu}(N\boldsymbol{t})'' + \boldsymbol{P}' \tag{23}$$

where as abbreviation

$$\boldsymbol{P} = \frac{\boldsymbol{f}}{\mu} - \nabla\Phi(\boldsymbol{r})$$

is introduced. Carrying out the differentiation of the products in (23) results in

$$\ddot{\eta}\boldsymbol{t} + 2\dot{\eta}\dot{\boldsymbol{t}} + \eta\ddot{\boldsymbol{t}} = \frac{1}{\mu}(N''\boldsymbol{t} + 2N'\boldsymbol{t}' + N\boldsymbol{t}'') + \boldsymbol{P}' \tag{24}$$

Projecting this equation in the direction of the tangent vector by taking the inner product of (24) with $\boldsymbol{t}$ and taking into account the relations $\boldsymbol{t}\cdot\dot{\boldsymbol{t}} = 0$, $\boldsymbol{t}\cdot\boldsymbol{t}' = 0$, $\boldsymbol{t}\cdot\boldsymbol{t}'' = -t'^2$ and $\boldsymbol{t}\cdot\ddot{\boldsymbol{t}} = -\dot{t}^2$ yields the fast equation for the elongation η

$$\ddot{\eta} - \eta\dot{t}^2 = \frac{1}{\mu}(N'' - Nt'^2) + \boldsymbol{P}'\cdot\boldsymbol{t}. \tag{25}$$

Equation (25) allows to eliminate the second derivative $\ddot{\eta}$ from (24) to obtain

$$\eta\ddot{\boldsymbol{t}} + 2\dot{\eta}\dot{\boldsymbol{t}} + \eta\dot{t}^2\boldsymbol{t} = \frac{N}{\mu}(\boldsymbol{t}'' + t'^2\boldsymbol{t}) + \left(\frac{N'}{\eta} + \left(\frac{N}{\eta}\right)'\right)\boldsymbol{t}' + \boldsymbol{P}' - (\boldsymbol{P}'\cdot\boldsymbol{t})\boldsymbol{t}. \tag{26}$$

which gives the required second equation. Eqs. (25) and (26) are equivalent to the original system (24) together with the constraint $\boldsymbol{t}\cdot\boldsymbol{t} = 1$. In fact we have one scalar equation (25) and one vector equation (26), which have to be solved. The limit to the inextensible tether can be performed setting $\eta = 1$ in (26) and (25). We note that the two equations (25) and (26) do not completely decouple but decouple only in the highest derivatives.

For the derivation of the corresponding boundary conditions, we refer to [3].

3. Numerical Treatment

In the numerical treatment of the equations of motion one can proceed in two directions. First starting from the equations of motion in strong form, either in displacement variables (1) or in natural string coordinates ((25) and (26)), one may perform a discretization based on Finite Differences. However, the equations of motion (19) in weak form are perfectly suited to perform a discretization by means of Finite Elements.

In both cases, however, we introduce first, following [24], a moving, but non-rotating reference frame, which moves on a prescribed orbit with vector $\boldsymbol{r}_R(t)$ in the neighborhood of the system (Figure 1). $\boldsymbol{r}_R(t)$ can be chosen arbitrarily, as long as the moving reference frame stays close enough to the system to avoid numerical problems due to small changes of large quantities. Hence the position vector $\boldsymbol{r}$ is split into two parts, describing the so-called nearfield $\boldsymbol{r}_T$ and farfield $\boldsymbol{r}_R$ dynamics. In general $\boldsymbol{r}_R(t)$ is chosen as the vector pointing to the mass center of the system. Second, since the length of the tether may vary, following [11] we transform the deployed tether length to the unit interval, to avoid time dependent Finite Elements (Figure 5). We obtain

$$\bar{s}\,(s,t) = \frac{s - s_{\mathrm{M}}\,(t)}{s_{\mathrm{S}}\,(t) - s_{\mathrm{M}}\,(t)} \in [0,1]\,,$$

however we will use s in the following expressions.

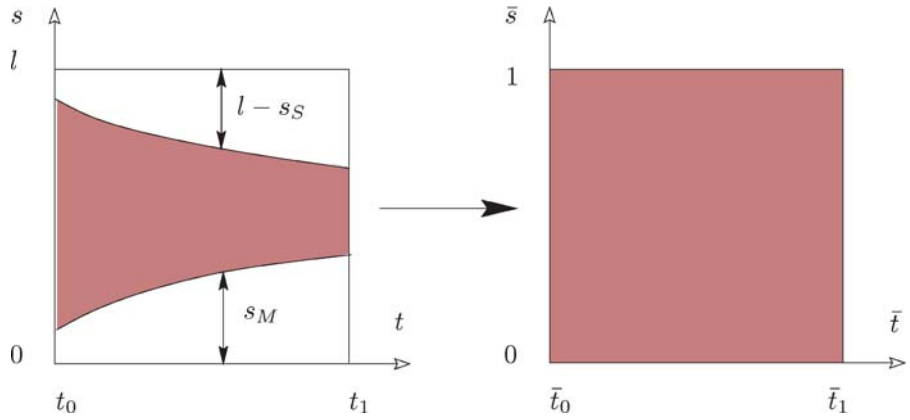

Figure 5. Transformation of the deployed tether length to a unit interval.

3.1. Weak Form of Equations of Motion

The weak formulation of the equations of motion is then given by a functional following from (19) which we write

$$G(\boldsymbol{x}(s,t), \boldsymbol{v}(s,t), \boldsymbol{a}(s,t), \delta\boldsymbol{x}(s,t)) = 0 \quad \forall \delta\boldsymbol{x}, \tag{27}$$

where $\boldsymbol{x}(s,t)$, $\boldsymbol{v}(s,t)$, $\boldsymbol{a}(s,t)$ and $\delta\boldsymbol{x}(s,t)$ stand for the position vector $\boldsymbol{r}_T(\bar{s},t)$, the two rotation matrices $\mathbf{B}_\mathrm{M}$, $\mathbf{B}_\mathrm{S}$ and the two arc-lengths $s_\mathrm{M}(t)$ and $s_\mathrm{S}(t)$ and their derivatives.

Now different solution approaches are possible. Following [25] we perform, first, a discretization in time of (27). This reverse order of discretization compared with the traditional approach is motivated in [25] by the argument that proceeding this way one is able to avoid having the details of the spatial discretization obscure the time integration of finite rotations which has to be performed for the motion of the endbodies. We recall that the update of the rotations is more complicated than the update of the displacements [25]. Introducing the spatial discretization first, the opinion expressed in [25] is that it would be more messy in the formulation. For problems with linear configuration spaces (e.g. small deformations), either approach is fine because they are equivalent. Moreover, the Newmark time integrator used in this approach turned out to be very efficient for the type of problems treated here. It is also in wide use for a number of other Finite Element calculations which were recently performed in [26, 27].

The discretization in time results in a nonlinear functional $\tilde{G}$ that is solved by means of the Newton–Raphson-method by a sequence of linearized problems of the form

$$\tilde{G}\big(\boldsymbol{u}_n^i, \delta\boldsymbol{x}\big) + D\tilde{G}\big(\boldsymbol{u}_n^i, \delta\boldsymbol{x}\big)\Delta\boldsymbol{u}_n^i = 0 \quad \forall \delta\boldsymbol{x}, \tag{28}$$

where $D\tilde{G}$ denotes the Frechet derivative of $\tilde{G}$.

To calculate a step in the Newton–Raphson method and find $\Delta\boldsymbol{u}_n^i$ we have to discretize all quantities which are still continuous in space. This discretization is performed by means of Finite Elements. The continuous tether is divided into a number of elements and the displacement inside an element is interpolated by ansatz-functions. Inserting cubic ansatz-functions and calculating the projections we finally obtain a system of linearized equations

$$\mathbf{K}\mathbf{c} + \mathbf{P} = 0,$$

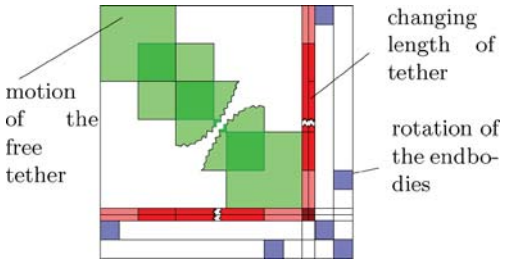

Figure 6. Arrow shaped stiffness matrix **K**.

where the vector **c** gives the nodal displacements. The structure of the matrix **K** is shown in (Figure 6). It has the form of an arrow matrix, where the arrow shape is a consequence of the changing mass composition of the system due to deployment or retrieval. For constant tether length the arrow shape disappears and the matrix has the indicated block diagonal form. The details of this approach are described in [13].

3.2. Strong Form of the Equations of Motion

For the equations of motion obtained from the strong formulation by means of a Finite Difference discretization we obtain a set of ordinary differntial equations which is of the form

$$\boldsymbol{A}(\boldsymbol{x}, t)\dot{\boldsymbol{x}} = \boldsymbol{g}(\boldsymbol{x}, t). \tag{29}$$

In the case of an inextensible cable the matrix $\boldsymbol{A}$ is singular and a so-called differential-algebraic system is obtained.

For the numerically stable integration in time of the set of ordinary differential equations (29) which are a stiff system in the mathematical sense, implicit methods must be used. In [22, 28] comparisons of different algorithms are given. Good results have been obtained with BDF methods possessing automatic step size-control and order-strategy like for example DASSL [29].

4. Simulation Results

In order to bring a system into operation, deployment of one satellite from another must be performed. This is an important but also delicate operation for a TSS mission because it leads to an unstable motion with respect to the stable radial relative equilibrium configuration of such a system, which is attained if it is moving with constant tether length on a Keplerian circle around the Earth. Therefore, if this deviation of the subsatellite from the local vertical is not desired, as it is the case for a reentry experiment, it is necessary to implement stabilizing control which usually is done by acting on the tension in the tether.

We present here first an uncontrolled deployment as it was performed in the SEDS mission by NASA and for which flight data exists with which we can compare our simulation results. Second we control the deployment process by an optimal control strategy. Strategies making use of the concept of controlling chaos are described in [30].

4.1. Uncontrolled Deployment

First we present simulation results for the case of free deployment which means that one of the forces, for example, N_M in (15) and (16) acting on the tether, where it leaves the satellite, either is zero or has a value determined by a brake. In contrast to the case of prescribed tether length, the arc-length $s_M(t)$ at the satellite, from which the tether is deployed, is an unknown variable.

We present a numerical simulation of the deployment in the small expendable deployer system (SEDS) mission. The SEDS project was conceived as a complement to the NASA tethered satellite system deployer for use when the tether retrieval is not required. Hence, tether storage is in a canister and not on a drum.

The two tethered satellite system missions SEDS-1 and SEDS-2 were successfully flown by NASA on March 29, 1993 and March 9, 1994 as secondary payloads on Delta II launches of GPS satellites [4]. The objectives of SEDS-1 were:

1. To demonstrate the capability of free deployment, that is to deploy a 20 km long tether, which is pulled out of the main satellite by the subsatellite due to Earth's gravity gradient;
2. bring the deployment to a smooth stop and;
3. when the payload swings through the local vertical, cut the tether and deorbit the payload of 25 kg from a low Earth orbit.

The initial momentum for the gravity gradient deployment to overcome dissipative effects is provided by a spring ejection system.

In Figure 7 real flight data of the SEDS-1 mission are presented. Especially the time dependence of the deploying tether length and also its velocity are presented in the two upper frames of Figure 7. With the data of the real mission, simulation results are presented in Figures 8 and 9, which were calculated with the simulation program. Comparing these results with the real flight data shows that good agreement has been achieved. In Figures 10 and 11 detailed plots of the motion of the subsatellite and the tether during deployment are shown. These results are presented in the orbital frame according to Figure 12. From Figures 10 and 11 it can be clearly seen that a strong deviation of the deploying subsatellite from the local vertical direction occurs. After the length change is finished the subsatellite starts to swing about the radial relative equilibrium and due to internal damping in the visco-elastic tether eventually will settle down in the local vertical configuration. But in a reentry mission as in the SEDS mission the tether will be cut when the subsatellite in its first back swing reaches the local vertical configuration.

4.2. Controlled Deployment

Obviously the free deployment considered above has the disadvantage that at the end of the tether length change a considerable deviation from the local vertical occurs. Moreover, the satellite does not come to a smooth stop. Both disadvantages can be avoided if the deployment process is controlled [30].

One possibility proposed in [10] is linear tension control making use of Kissel's law.

Another possibility is optimal control applying Pontrijagin's Maximum Principle [31]. In [31] a finite dimensional system of a space pendulum (Figure 13) is considered with 2 degrees of freedom φ, ξ. We present as example the simple case of the time optimal control problem:

For given initial and final values of the variables $\boldsymbol{q} = (\varphi, \dot{\varphi}, \xi, \dot{\xi})$, *find the control function* $u(t) \in [u_{\min}, u_{\max}]$, *which minimizes the performance functional*

$$I = \int_0^T F(\boldsymbol{q}(t))\, dt = \int_0^T dt. \tag{30}$$

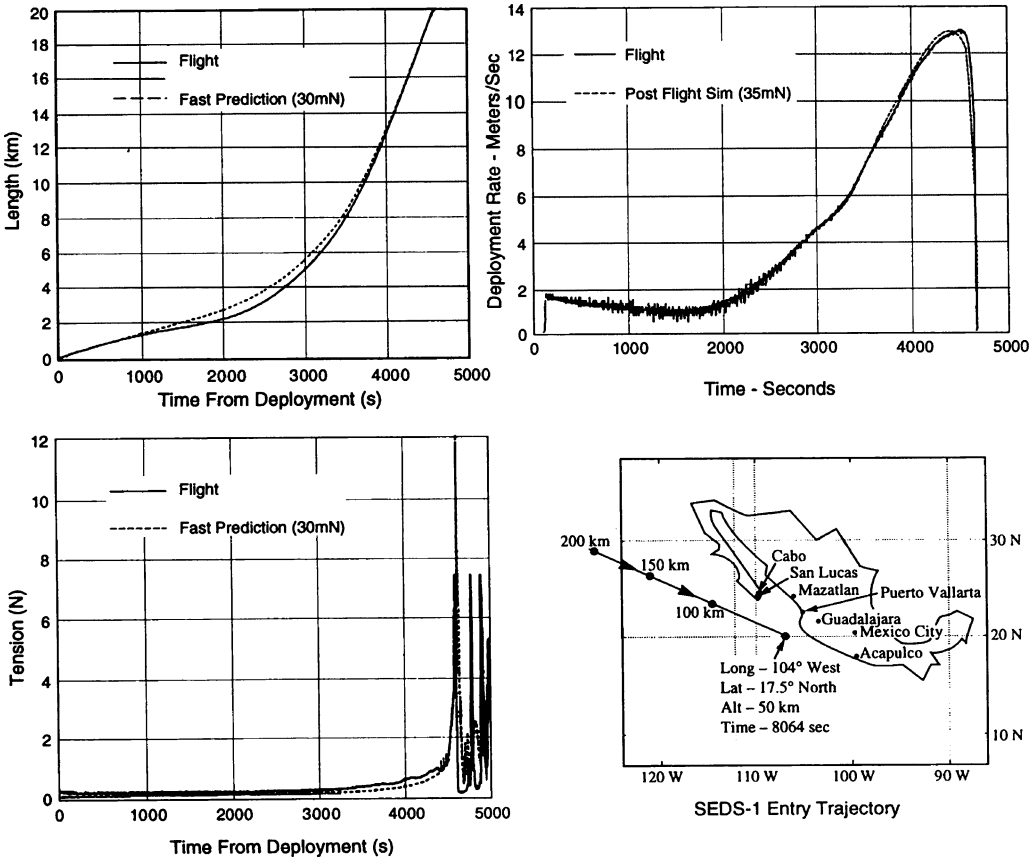

Figure 7. Real flight data for SEDS-1 from H. F. Smith (NASA) [4].

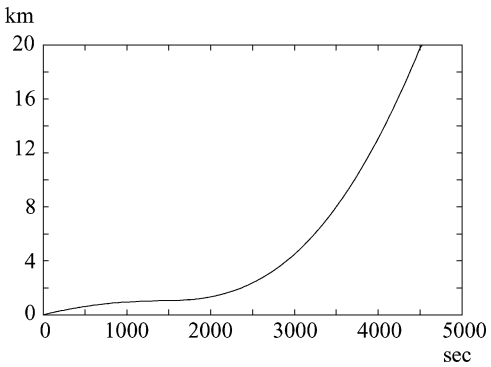

Figure 8. Computed tether length (km) vs. deployment time to be compared with the measured flight data of Figure 7.

The detailed treatment of this problem and of more general problems, where constraints like the deviation from the radial position and the monotonicity of deployment are also included, are given in [31].

As typical for such problems a bang-bang-solution is obtained. For a tether length ratio $\xi_0/\xi_T = 1/20$ one obtains a time optimal solution with three switching points given by the zeros of the adjoint variable as depicted in the left frame of Figure 14. The corresponding control function is depicted in the right

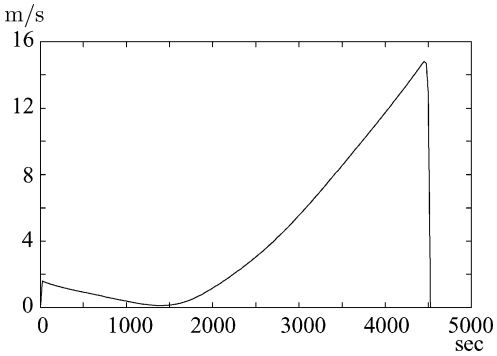

Figure 9. As in Figure 8, but deployment rate (m/s) vs. deployment time.

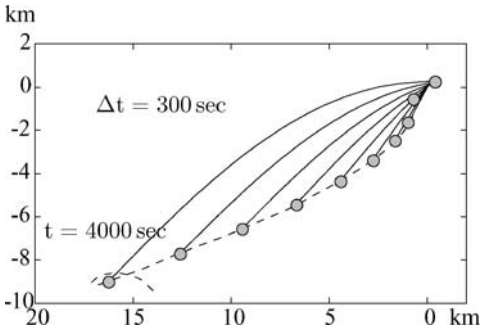

Figure 10. Simulation of the deploying subsatellite relative to the main satellite in the SEDS mission for $0 \leq t \leq 4000$.

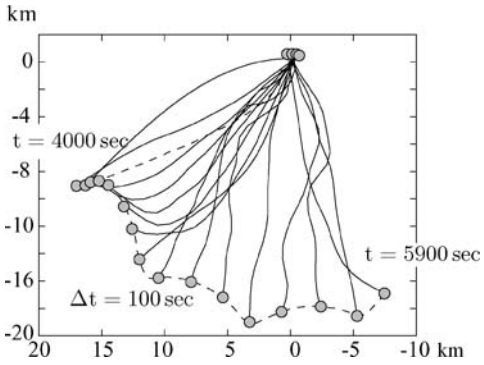

Figure 11. Continuation of the motion of Figure 10 for $4000 \leq t \leq 5900$.

frame of Figure 14 showing clearly the "bang-bang" character of the control u (dimensionless tether force) switching between $u_{\min} = 0$ and $u_{\max} = 3.15$.

The corresponding time optimal orbit, represented in the orbital frame (Figure 12) is depicted in Figure 15. The different control strategies are marked by varying the line types of the orbit.

The strategy works fine for the simplified model of the tethered satellite system. Since for a real system a flexible massive tether joins the two satellites we now want to show whether the strategy developed for the massless tether model can be of practical use for the system with massive tether. For this purpose, we implement the optimal control strategy into the computer code described above based on the finite element discretization for a massive tether model.

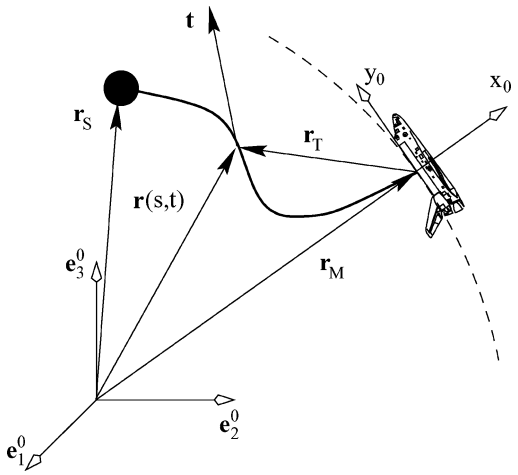

Figure 12. For the presentation of simulation results the rotating orbital frame x_0, y_0, z_0 is most convenient.

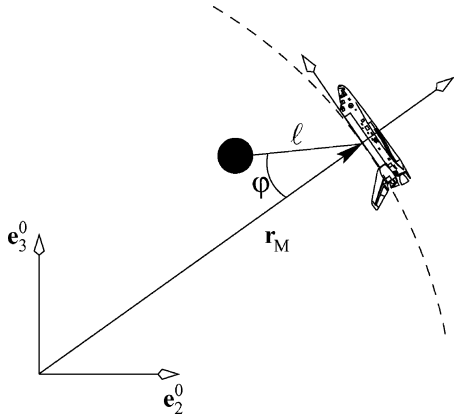

Figure 13. Simplified model of a space pendulum for the optimal control problem.

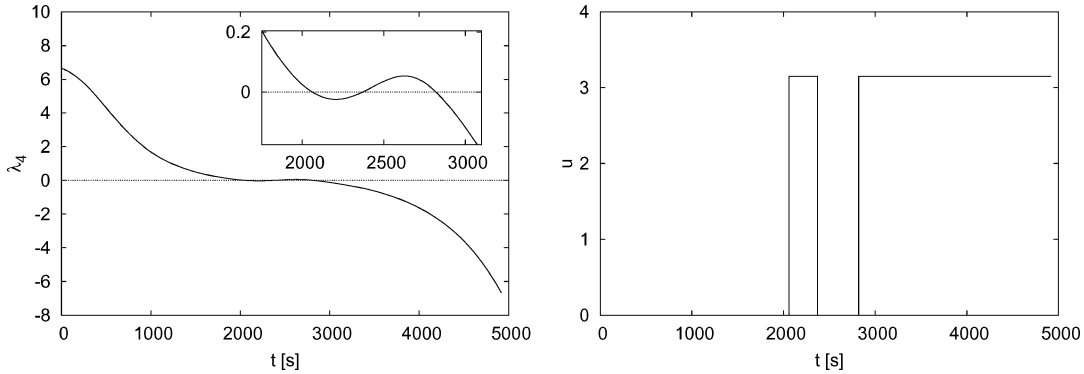

Figure 14. Left frame: switching function $\lambda_4(t)$ of the time optimal solution for the initial condition $\xi_0 = 0.05$. Right frame: corresponding bang-bang control function $u(t)$ with three switching points.

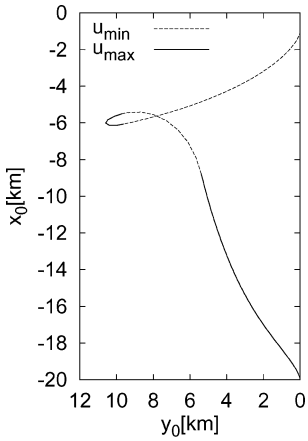

Figure 15. Trajectory of the subsatellite for the time optimal solution of Figure 14 for the massless tether model of Figure 13 in the orbital frame shown in Figure 12.

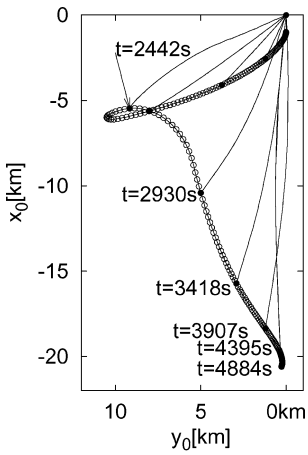

Figure 16. Simulation of the deployment for the massive tether model corresponding to the three switching points of Figure 15. Data: $\ell_0 = 1$ km, $\ell_T = 20$ km.

The switching intervals obtained for the massless tether system are taken as inputs for the simulation of the continuous massive tether system. The flight path of the subsatellite with the massive tether shown in Figure 16 follows the trajectory of the simpler optimal control model given in Figure 15 quite closely.

Finally, to give the reader some feeling, we give two numbers. First, we consider free uncontrolled deployment. The initial position of the subsatellite is as in Figure 16 the radial relative equilibrium position 1 km below the space ship. The deployment process is stopped when 20 km of tether are deployed. For a subsatellite of 1000 kg mass and a tether mass of 1 kg/km we obtain $T = 2650$ s. However, the system configuration is far away from the radial relative equilibrium and large amplitude oscillations [13] are starting. The optimal steering process shown in Figure 16 takes $T = 4884$ s. However, now the system is again in the radial relative equilibrium position whereas after free deployment other control actions would have to be used to steer the system into its stable radial relative equilibrium. Control strategies that make use of the concept of controlling chaos to achieve this goal are described in [30].

That the controlled motion of the continuous system, which is governed by a set of partial differential equations, is so close to the optimally controlled motion of the simple finite dimensional system is surprising at the first glance. But plausible explanations are first that the control action on the system by tension control is practically the same for both systems and is effective for the system with massive tether only if the tether is stretched. Moreover, the mass of the tether is much smaller than the mass of the satellites.

4.3. Comparison Between Displacement and Natural Coordinates

In a comparison of the two alternative formulations (Figure 4) besides speed of integration also accuracy and the ability to continue the integration for a long time interval is important. The second point means that especially in those phases of the motion of the tethered satellite system, when the tether is not under tension, the tether becomes slack which results in configurations that caused some of the programs to stop the integration. Here it turned out that the formulation in natural variables was much better than the one in displacement variables. Moreover for the natural variables a smoother configuration of the tether is obtained than for the displacement variables. The difference in CPU-time for the different formulations is clearly visible from Figure 17. For the CPU time comparison we scaled such that the tether stiffness $EA = 10^4$ results in CPU $= 1$.

Without any doubt the formulation in natural coordinates is not only more efficient numerically but also smoother configurations of the string are obtained in case the string becomes slack. However we have to note that the formulation in the natural coordinates is more complicated and requires greater theoretical efforts. For more details see [22].

4.4. Stability of Relative Equilibria

Relative equilibria exist in symmetric Hamiltonian systems and are equilibria in properly moving coordinate frames, for example in the orbit frame of Figure 12. Expressing this fact more mathematically: *For a relative equilibrium the dynamic orbit of the system coincides with a one-parameter group orbit of the symmetry group of the system.*

The most interesting relative equilibrium, from the application's point of view, is the *radial* relative equilibrium Figure 18(a). This relative equilibrium exists for freely moving end bodies and is stable provided the tether length is not too long [3]. In [3] it is also shown, that under the assumption of constant thrust forces acting on the end bodies, there exist relative equilibria with wavy configurations

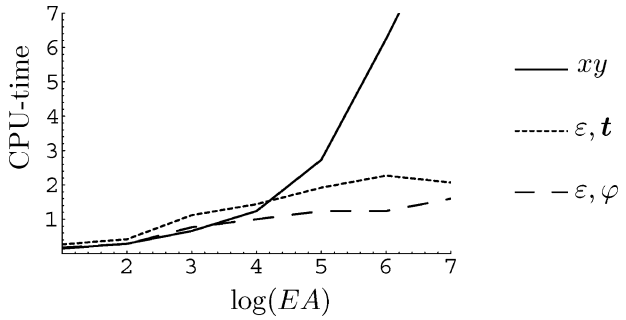

Figure 17. CPU-time as a function of the string stiffness EA for three formulations: Displacement variables, $\varepsilon, \boldsymbol{t}$ and ε, φ. As time integrator DASSL [29] is used.

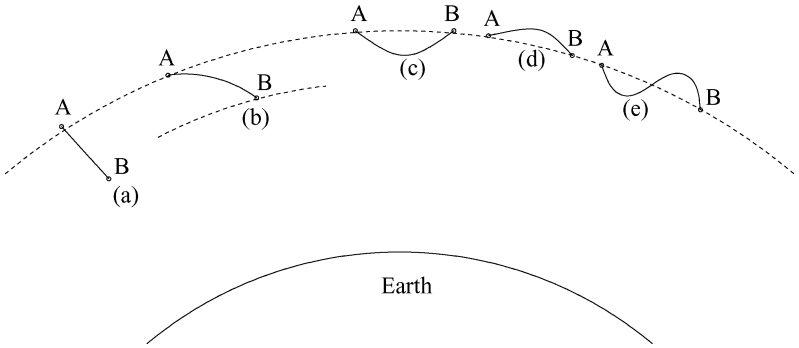

Figure 18. Examples of relative equilibria of a tether system: (a) radial; (b)–(e) wavy.

of the tether, as shown in Figure 18(b)–(e). In [3] it is assumed, in order to maintain the conservative structure of the problem, that the forces of thrust acting on the end bodies are constant and equal to the ones necessary for the relative equilibrium to exist. Under these constant force assumptions the stability results are rather restrictive; a relative equilibrium is not stable unless the distance of a point on the tether from the Earth is a monotone function of the arc-length as for example in Figure 18(b). The configurations of Figure 18(c)–(e) are unstable under this assumption.

We consider a slightly different problem. We assume that satellite A is moving on a circular Keplerian orbit which is not perturbed by the motion of satellite B which moves on a vertical line relative to satellite A. This is shown in Figure 19, where satellite A always stays in the origin of the coordinate frame and satellite B starting in position 0 moves upwards. The problem we study is whether the resulting planar nontrivial configuration of the tether corresponds to a stable state. This question is answered by means of the reduced energy momentum method [6, 7, 8] by checking the second derivative of the amended potential

$$V_{\mu_e}(\boldsymbol{q}) = V(\boldsymbol{q}) + \frac{1}{2}\mu_e \cdot I(\boldsymbol{q})^{-1}\mu_e \tag{31}$$

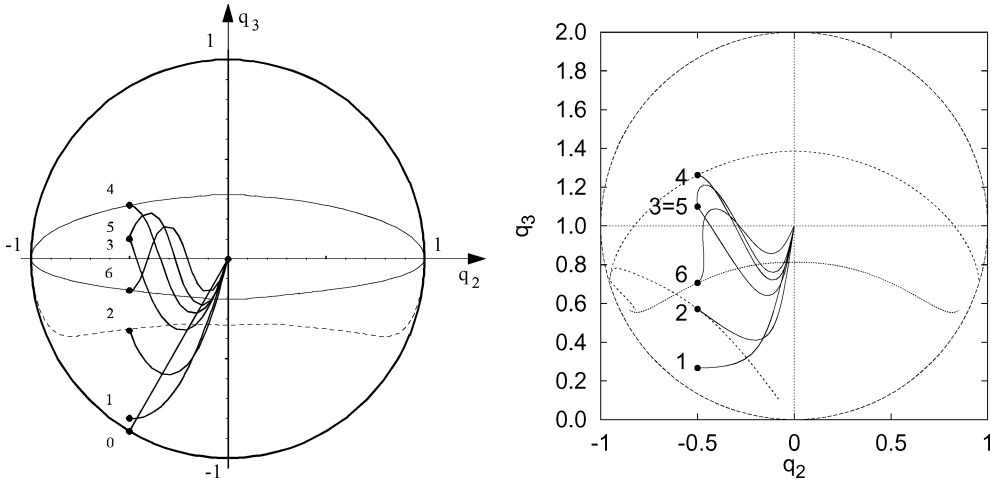

Figure 19. Relative equilibria as a function of the position of the satellite B. The left figure shows the shapes of an inextensible tether in a linearized force field, corresponding to a small tether length $\ell \ll |\boldsymbol{r}_A|$. The right figure shows the corresponding shapes of an inextensible extremely long tether $\ell = |\boldsymbol{r}_A|$.

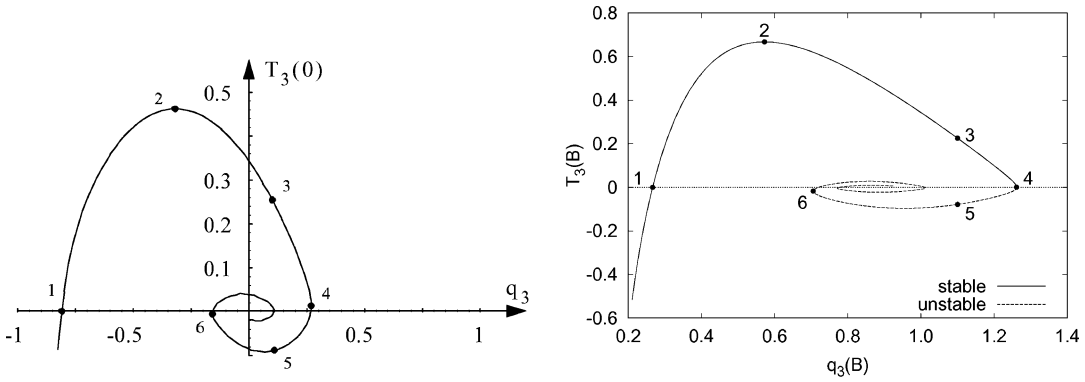

Figure 20. Vertical coordinate q_3 related to the force in the vertical direction at B corresponding to Figure 19.

for positive definitness. In (31) $V(\boldsymbol{q})$ is the potential given in (18), μ_e the angular momentum of the relative equilibrium configuration and $I(\boldsymbol{q})$ is the inertia tensor of the system locked in the relative equilibrium. The nontrivial calculations necessary to prove definiteness are performed in [32].

For a quasi-static movement of satellite B (points 0–6) the planar shapes of the relative equilibria are depicted in Figure 19 left frame for a short tether ($\ell \ll |\boldsymbol{r}_A|$) and in Figure 19 right frame for a long tether ($\ell \sim |\boldsymbol{r}_A|$). Let T be the force necessary to sustain the relative equilibrium. Figure 20 shows the relation between the vertical component T_3 of this force and the vertical coordinate q_3. Points 1–6 marked on the graphs in the left and right frames of Figure 20 correspond to the positions 1–6 in the left and right frames of Figure 19.

Continuation of the relative equilibrium from an almost straight configuration leads first to position 1, where the force in the vertical direction T_3 changes sign. Point 2 corresponds to the maximum of T_3. Further continuation leads to point 4 marking the maximum of the vertical coordinate q_3 for the family of relative equilibria. Beyond point 4 the relative equilibrium has a wave-like configuration. At point 6 the curve in Figure 20 has another turning point corresponding to the appearence of the next hump in the wave form of the relative equilibrium. By continuing this process waves with arbitrary many humps can be found.

Note that for some regions of the q_3 values there exist multiple solutions with the same q_3 value. An example is given by the coincident points 3 and 5.

We remark that there exists also a second family of relative equilibria which are curved upwards. In the left frame of Figure 19 they are obtained by reflecting the depicted solutions about the abszissa. The curve in Figure 20 corresponding to these solutions is obtained by rotating the depicted curve by π.

The evaluation of the stability condition in [32] shows that the relative equilibria up to point 4 are stable. If one proceeds above point 4 only the second solution family, mentioned above, exists. Going down to point 5 two configurations exist. Only the one which is without second hump is stable. This is also true for the more complicated wavy forms, which are all unstable.

4.5. Chaotic Dynamics

Figure 21 shows four relative equilibria of a tethered satellite system under the only influence of the gravitational field of the Earth which is supposed to be an homogenous sphere. We call them relative equilibria since all points of the tether and the satellites A and B are moving on concentric circles with equal angular rate. It is well known that the two radial configurations are stable, whereas the two

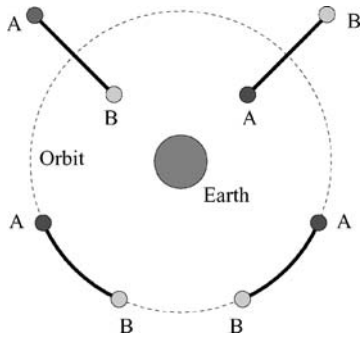

Figure 21. Stable and unstable equilibria of a tethered satellite system on a circular orbit.

tangent-to-orbit equilibria are unstable. Now we ask in which of the stable equilibria the internally damped system settles down finally, in particular, if we start in the neighborhood of an unstable configuration. Since we are dealing with a highly nonlinear, nearly Hamiltonian multiple degree of freedom system, we might expect for large amplitude motions transient chaotic behaviour, because slight dissipation will not destroy (unstable) hyperbolic equilibria. It will however transform stable elliptic equilibria into asymptotically stable ones. Damping is introduced in our system by the visco-elastic Kelvin–Voigt material-law (4).

For the following simulations we choose a tether of 100 m length with $EA = 5000$ N and a damping parameter $\alpha = 0.01$ s. The initial configuration is shown in Figure 22. The initial tether-shape was calculated as relative equilibrium for both satellites moving on a prescribed circular Keplerian orbit. The distance d_0 between A and B slightly differs from the distance in the unstable tangent-to-orbit equilibria of Figure 21. So, for keeping this initial configuration the position of the endbodies must be controlled by appropriate thrusts. After switching off these thrusts the system performs very complex transient motions in the orbital plane and finally approaches one of the stable equilibria of Figure 21.

Figure 23 shows the pitch-angle between the connecting line of the two satellites and the local vertical through the system's center of mass and the center of Earth. During the first 10 000 s the three curves, corresponding to slightly differing values of d_0, are very close together but after one rotation they separate and settle down in librations around one of the stable equilibria. The amplitudes of these final oscillations decrease only very slowly since there exists one pair of eigenvalues which is located closely to the imaginary axis. Physically speaking, there is only very weak influence of axial damping on transversal oscillations.

Performing simulations for several values of d_0 in the range of 98.98 to 99.03 m we can observe a sensitive dependence of the asymptotic behaviour on the initial condition. The following table shows the final equilibrium as a function of d_0:

d_0 (m)	98.98	98.99	99.00	99.01	99.02	99.03
Upper satellite	B	A	B	A	A	B

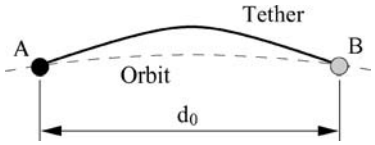

Figure 22. Inital configuration close to the unstable tangent-to-orbit equilibria of Figure 21.

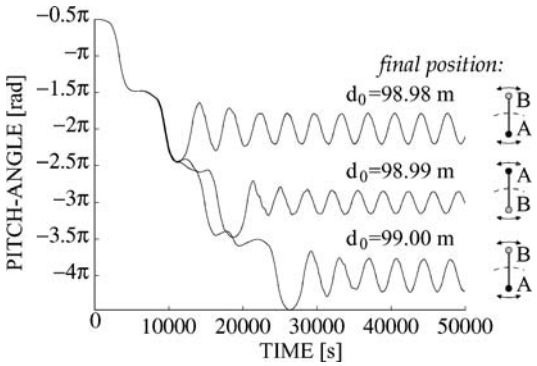

Figure 23. Pitch-angle vs. time for three slightly differring values of d_0.

Thus, for $d_0 = 99.00\,\text{m}$ we obtain satellite B to be the upper one, but decreasing d_0 by just 10 mm we end up with satellite B as the lower one. However, for $d_0 = 98.98\,\text{m}$ the situation is again reversed.

The existence of solutions sensitive to small changes of the initial conditions implies a certain restriction to the reliability of numerical calculations. Thus, we may ask: How does the basin boundary of the stable equilibria look like? Can we expect a fractal nature of this boundary so that it is impossible to predict the long-time behaviour of a tethered satellite system for initial conditions in its vicinity? The investigation of a large number of initial conditions necessary to answer these questions requires a much simpler model. Such a model, the so-called space billard, is treated in [3, 33]. There it is shown that the domain of attraction possesses a fractal boundary.

5. Conclusions

We hope that the reader got some feeling that tethered satellite systems are not only an important concept for space flight but also are a mechanical system that poses interesting problems. Some of these problems have been addressed, like modelling of a hybrid mechanical system consisting of continuous deformable and rigid bodies, derivation of equations of motion in weak form, numerical solution strategies for a mathematically stiff system of equations, control of deployment, stability of relative equilibria and chaotic dynamics.

As always for such complex problems one is faced with the fact that if one question is answered immediately new questions arise. Some of these are: is the modelling of the tether by a string adequate or should small bending stiffness be included, possibly treating the problem as a singular perturbed system? Is the practically important structural damping adequately described by the linear visco-elastic material law or should a more complicated law be considered? The modelling of tether storage, especially if retrieval of the tether should be possible, still must be considerably improved. The system dynamics under other environmental influences (air drag, electro-magnetic forces, solar pressure) should be investigated. Another important point would be to ask for three-dimensional relative equilibria. Finally we mention that tethered satellite systems consisting of more than two satellites should also be treated. Here the simplest case would be to include a third satellite moving up and down the tether of a system which is moving in the radial relative equilibrium position. Such a satellite could be used as a microgravity laboratorium.

Acknowledgements

The financial support of this work by the Austrian Science Foundation (FWF) under project P-15825 is gratefully acknowledged. We also thank the reviewer for his comments which helped to improve the paper.

References

1. P. M. Bainum, I. Bekey, L. Guerriero, P. A. Penzo (eds.), *Handbook: Tethers in Space*, *Advances in the Astronautical Sciences*, **62**, American Astronautical Society, 1986.
2. *Handbook: Space Tethers for Science in the Space Station Era*, Societa Italiana di Fisica, Conference Proceedings, **14**, Bologna, 1988.
3. Beletskii, V. V. and Levin, E. M., 'Dynamics of space tether systems', *Advances of the Astronautical Sciences* **83**, 1993, 267–322.
4. *Proceedings of the Fourth International Conference on Tethers in Space*, Smithsonian Institution, Washington, D.C., 10–14 April 1995, Science and Technology Corporation, Hampton, VA, 1995.
5. Simo, J. C. and Lewis, D., 'Energy methods in the stability analysis of relative equilibria of Hamiltonian systems', in *Proceedings of the Sixth Symposium on Continuum Models and Discrete Systems*, Dijon, June 1989, G. A. Maugin (ed.), Longman, 1989, pp. 162–183.
6. Marsden, J. E. and Ratiu, T. S., *An Introduction to Mechanics and Symmetry, A Basic Exposition of Classical Mechanical Systems*, Springer-Verlag, New York, 1994.
7. Simo, J. C., Lewis, D., and Marsden, J. E., 'Stability of relative equilibria. Part I: The reduced energy-momentum method', *Archive for Rational Mechanics and Analysis* **115**, 1991, 15–59.
8. Simo, J. C., Posbergh, T. A., and Marsden, J. E., 'Stability of relative equilibria. Part II: Application to nonlinear elasticity', *Archive for Rational Mechanics and Analysis* **115**, 1991, 61–100.
9. Bainum, P. and Kumar, V. K., 'Optimal control of the shuttle-tethered-subsatellite system', *Acta Astronautica* **7**, 1980, 1333–1348.
10. Misra, A. K. and Modi, V. J., 'Deployment and retrival of shuttle supported tethered satellites', *Journal of Guidance and Control* **5**(3), 1982, 278–285.
11. Kohler, P., Maag, W., Wehrli, R., Weber, R., and Brauchli, H., *Dynamics of a System of two Satellites Connected by a Deployable and Extensible Tether of Finite Mass*, ESTEC Contract No. 2992/76/NL/AK(SC), 1978.
12. Steiner, W., Steindl, A., and Troger, H., 'Dynamics of a space tethered satellite system with two rigid endbodies', in *Proceedings of the Fourth International Conference on Tethers in Space*, Science and Technology Corporation, Hampton, VA, 1995, pp. 1367–1379.
13. Wiedermann, G., Schagerl, M., Steindl, A., and Troger, H., 'Computation of force controlled deployment and retrieval of a tethered satellite system by the finite element method', in *Proceedings of ECCM'99*, W. Wunderlich (ed.), 1999, pp. 410–429.
14. Schagerl, M., Troger, H., and Wiedermann, G., 'Boundary conditions for the cable dynamics of tethered satellite systems', in *Proceedings of the Third International Symposium on Cable Dynamics*, Trondheim, 1999.
15. Krupa, M., Kuhn, A., Poth, W., Schagerl, M., Steindl, A., Steiner, W., Troger, H., and Wiedermann, G., 'Tethered satellite systems: A new concept of space flight', *European Journal of Mechanics A Solids* **19**(special issue), 2000, S145–S164.
16. Arnold, V. I., *Mathematical Methods of Classical Mechanics*, Springer-Verlag, New York, 1978.
17. Schagerl, M., Steindl, A., and Troger, H., 'Dynamical analysis of the deployment process of tethered satellite systems', in *Proceedings of the IUTAM/IASS Symposium on Deployable Structures: Theory and Application*, S. Pellegrino, S. D. Guest (eds.), *Solid Mechanics and its Applications*, 80, Kluwer Academic Publishers, Dordrecht, 2000, pp. 345–354.
18. Crellin, E. B., Janssens, F., Poelaert, D., Steiner, W., and Troger, H., 'On balance and variational formulations of the equations of motion of a body deploying along a cable', *Journal of Applied Mechanics* **64**, 1997, 369–374.
19. Lur'e, L., *Méchanique Analytique*, Vol. I & II, Masson & Cie, Paris, 1968.
20. Sommerfeld, A., *Vorlesungen über Theoretische Physik, Vol. 1, Mechanik*, Akademische Verlagsgesellschaft Leipzig, 1943, p. 249.
21. Hairer, E. and Wanner, G., *Solving Ordinary Differential Equations, II. Stiff and Differential-Algebraic Problems*, Springer Verlag, Berlin, 1991.
22. Poth, W., Matzl, P. W., Auzinger, M., Steindl, A., and Troger, H., 'Comparison of displacement versus natural variables for the numerical simulation of a string pendulum, nonlinear dynamics, chaos, control and their applications to engineering sciences', in *Vol. 5: Chaos, Control and Time Series*, J. M. Balthazar, P. B. Goncalves, R. F. Brasil, I. L. Caldas, and F. B. Rizatto (eds.), 2002, pp. 127–136 (ISBN 85-900351-5-8).

23. Kuhn, A., 'Numerische Behandlung von "Tethered Satellite Systems" unter besonderer Berücksichtigung längssteifer Verbindungsseile', Dissertation TU-Wien, 1995.
24. Vu-Quoc, L. and Simo, J. C., 'Dynamics of Earth-orbiting flexible satellites with multibody components', *Journal of Guidance, Control and Dynamics* **10**, 1987, 549–558.
25. Simo, J. C. and Vu-Quoc, L., 'On the dynamics in space of rods undergoing large motions – A geometrically exact approach', *Computer Methods in Applied Mechanics and Engineering* **66**, 1986, 125–161.
26. Kane, C., Repetto, E. A., Ortiz, M., and Marsden, J., 'Finite element analysis of nonsmooth contact', *Computer Methods in Applied Mechanics and Engineering* **180**, 1999, 1–26.
27. Kane, C., Marsden, J. E., and Ortiz, M., 'Symplectic energy momentum integrators', *Journal of Mathematical Physics* **40**, 1999, 3353–3371.
28. Poth, W., Schagerl, M., Steindl, A., Steiner, W., and Troger, H., 'Numerically efficient formulation of the equations of motion of tethered satellite systems', in *Proceedings of IUTAM Symposium on Discretization Methods*, Vienna, 1997.
29. Brenan, K. E., Cambell, S. L., and Petzold, L. R., *Numerical Solution of Initial-Value Problems in Differential-Algebraic Equations*, North Holland, New York, 1989.
30. Barkow, B., Steindl, A., Troger, H., and Wiedermann, G., 'Various methods of controlling the deployment of a tethered satellite', *Journal of Vibration and Control* **9**, 2003, 187–208.
31. Steindl, A. and Troger, H., 'Optimal control of deployment of a tethered subsatellite', *Nonlinear Dynamics* **31**, 2003, 257–274.
32. Krupa, M., Schagerl, M., Steindl, A., Szmolyan, P., and Troger, H., 'Relative equilibria of tethered satellite systems and their stability for very stiff tethers', *Dynamical Systems* **16**, 2001, 253–287.
33. Steiner, W., 'Transient chaotic oscillations of a tethered satellite system', *Acta Mechanica* **127**, 1998, 155–163.
34. Beardsley, T., 'The way to go in space', Scientific American, February, 1999.
35. Hoyt, R. P., Forward, R. L., Nordley, G. D., and Uphoff, C. W., 'Rapid interplanetary tether transport systems, IAF-99-A.5.10', in *Proceedings of the 50th IAF Congress*, Amsterdam, 1999, 31 pp.
36. Marsden, J. E., *Lectures on Mechanics*, London Mathematical Society, Lecture Note Series 174, Cambridge University Press, Cambridge, 1992.
37. Zimmermann, F., Schoettle, U. M., and Messerschmid, E., 'Optimal Deployment and return trajectories for a tether-assisted re-entry mission', in *Proceedings of the AIAA 99-4168, AIAA Atmospheric Flight Mechanics Conference*, Portland, OR, August 9–11, 1999.